Flow Vectors Around an Escort Tug at a Large Yaw Angle

David Molyneux[1], Jie Xu[2] and Neil Bose[3]

[1]*Institute for Ocean Technology, National Research Council Canada*
St. John's, NL, A1B 3T5, Canada

[2]*Faculty of Engineering and Applied Science, Memorial University of Newfoundland*
St. John's, NL, A1B 3X5, Canada

[3]*Australian Maritime College, Launceston, Tasmania, 7250, Australia*

Email:David.Molyneux@nrc-cnrc.gc.ca

ABSTRACT

The flow around a ship at yaw angles beyond those encountered during manoeuvres has not been the subject of much research reported in the literature. These conditions are particularly important for an escort tug, since it uses large yaw angles to generate hydrodynamic forces that are used to control a ship (normally a tanker) in the event of an emergency. This paper presents CFD predictions for the flow around an escort tug at a yaw angle of 45 degrees and compares them to PIV measurements of the flow patterns. The CFD code predicts the essential features measured within the flow, such as the separation of the flow from the upstream bilge, and the formation of a large vortex generated by the low aspect ratio fin. The predicted vectors were compared with the measured ones using a numerical technique, and the agreements were found, on average, to be within 10%. This level of agreement was within the estimated uncertainty of the PIV system used for the experiments.

1. INTRODUCTION

An escort tug is an extreme example of a small ship operating in 'off-design' hydrodynamic conditions. The tug uses its hull and propulsion system to create a hydrodynamic force, which is used to control a loaded ship (usually an oil tanker) in an emergency. The tug is attached to a towline at the stern of the tanker, and by using vectored thrust, it is held at a yaw angle of approximately 45 degrees [1, 2, 3]. The maximum practical speed of operation for escort tugs is about 10 knots, corresponding to a maximum Froude number based on ship length of around 0.30 for a tug approximately 40 m long.

Escort tug research to date [1, 2, 3] has focused on predicting the total force and the limits of safe operation for specific combinations of hull and propulsion system using physical model experiments. The problem has not been approached from the point of view of trying to analyze the hydrodynamics of the situation and its influence on the resulting solution.

One method of trying to understand the flow around a hull with a large yaw angle is to use computational fluid dynamics (CFD). The basic equations of fluid motion can be combined with the hull geometry and some assumptions about the turbulence in the flow to give mathematical predictions of the pressure on the hull surface and the flow vectors within the fluid. Very little numerical analysis has been carried out on the hydrodynamics of hull shapes designed to operate at large yaw angles, and so the accuracy of CFD in these situations is unknown. A validated CFD code can give insights into the flow around a hull at a large yaw angle, without the need for physical model experiments.

This paper presents a CFD simulation of the flow vectors around an escort tug operating at 45 degrees of yaw, and compares these predictions with experimental measurements of the flow for the same conditions, using Particle Image Velocimetry (PIV).

2. CFD PREDICTIONS OF FLOW VECTORS

The hull chosen for the research described in this paper was a concept for a tractor tug developed by Robert Allan Ltd. of Vancouver, B. C. [2]. The model had been previously tested at the NRC Institute for Ocean Technology (IOT). Force measurements were made at several speeds for a range of yaw angles from zero to 105 degrees [4]. When the measured force values were non-dimensionalized, the results for all speeds reduced to small variations about a mean value of force coefficient. This implied that free surface wave effects were small for the range of speeds typically found in escort tug operation. This observation simplified the CFD predictions since only the hull below the design waterline needed to be considered, and the free surface effects could be ignored.

A summary of the tug model geometry is given in Table 1. For this study the model was always moving with the fin going forwards (although the ship is actually going astern based on conventional definitions of bow and stern).

Table 1, Summary of model particulars

Length, waterline, m	2.122
Beam, waterline, m	0.789
Draft, hull, m	0.211
Daft, maximum, m	0.471
Displacement, kg	213.3
Nominal scale	1:18

The flow patterns were predicted for a typical operating condition for an escort tug in 'indirect' mode, described in Table 2.

The hull geometry, up to the level of the waterline was meshed using *GAMBIT* [5]. The mesh was re-scaled in *FLUENT* [6] to have units of metres, model scale and an origin at the leading edge of the waterline for the hull.

Table 2, Yaw angles and speeds tested

Yaw angle, deg	Model speed, m/s	Ship speed, knots
45	0.5	4.12
45	1.0	8.24

A rectangular 'tank' was constructed around the hull. This had to be a compromise between being large enough that the boundaries had little effect on the results, and small enough that the numerical solution converged in a reasonable time. A mesh sensitivity study showed that the number of elements in the mesh did not significantly affect the predicted force. The total number of elements within the mesh used for results given in this paper was 986,984. The mesh close to the hull is shown in Figure 1. A summary of the volume of fluid used as the domain is given in Table 3.

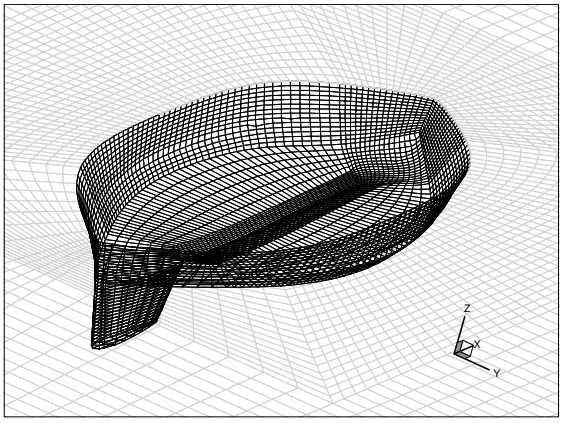

Figure 1, Mesh for escort tug with fin.

Table 3, Summary of domain dimensions

x_{max}	x_{min}	y_{max}	y_{min}	z_{max}	z_{min}
m	m	m	m	m	m
7.974	-2.059	4.318	-4.318	0.000	-2.159

The boundary conditions were set as velocity inlets on the two upstream faces, and pressure outlets at the two downstream faces. The upper and lower boundaries were set as walls with zero shear force. The hull surface was set as a no-slip wall boundary condition.

The CFD solver used was *FLUENT 6.1.22*. Uniform flow entered the domain through a velocity inlet on the upstream boundaries and exited through a pressure outlet on the downstream boundaries.

The angle between the incoming flow and the hull (yaw angle) was set by adjusting the boundary conditions, so that the velocity at the inlet planes had two components. The cosine component of the angle between the steady flow and the centreline of the hull was in the positive *x* direction for the mesh and the sine component in the positive *y* direction. The pressure outlet planes were set so that the backflow pressure was also in the same direction. The advantage of this approach was that one mesh could be used for all the yaw angles. Yaw angles from 10 degrees to 45 degrees were simulated.

The turbulence model used was a κ–ω model with *FLUENT's* default parameters. Turbulence intensity and turbulent viscosity ratios were set at 1% and 1 respectively. The flow was solved for the steady state case. The non-dimensional residual for each of the solution variables (continuity, *x, y* and *z* velocity components, κ and ω) were set to 10^{-3} (default values). All flow conditions reported came to a solution within these tolerances.

3. PARTICLE IMAGE VELOCIMETRY MEASUREMENTS OF FLOW VECTORS

In order to check the accuracy of the CFD predictions, it was necessary to obtain experimental measurements for the same flow conditions. In January 2004, Memorial University purchased a Particle Image Velocimetry system for making flow measurements in a towing tank. Xu et al. presented a description of the system [7]. This system consists of two CCD cameras mounted at the top of borescopes, a laser with optics to make a plane of light under the water surface and a computer for control of the components and data acquisisition.

Molyneux et al. [8] gave an estimate of the uncertainty of the system in the configuration used for the experiments described in this paper, which was shown to be between 8% of the undisturbed flow speed at 1 m/s and 16% at 0.5 m/s.

Key locations were selected for comparing the results of experiments with the CFD predictions. These were taken as planes normal to the undisturbed flow, intersecting with the hull on the upstream and downstream sides. These are shown in Figure 2.

To reduce the corruption of recorded images by reflected laser light, the hull was painted matt black. Contrasting targets, made from narrow yellow strips of tape were placed at key locations on the model. These were used to align the laser beam, to ensure that it was at the required position relative to the model.

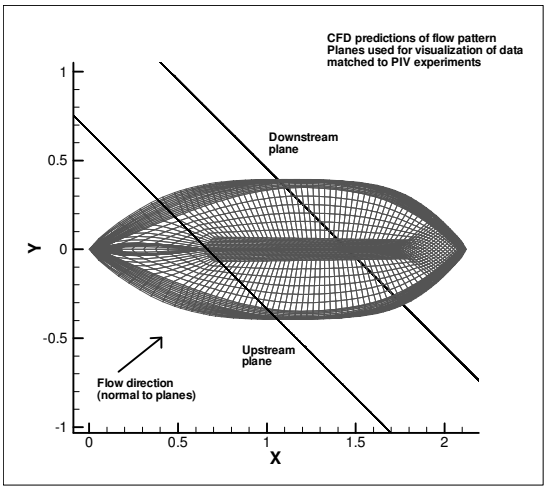

Figure 2, Planes used for comparison on CFD predictions and measurements of flow vectors.

The PIV measurements were carried out in the Ice Tank of the National Research Council's Institute for Ocean Technology. The carriage included a test frame, which was adjustable vertically and had two longitudinal beams that can be moved independently while remaining parallel to the centreline. This adjustment feature was used to vary the location of the measurement window, relative to the model. Each beam had a scale so that the exact locations of the beam, relative to the centreline of the test frame were known. The PIV equipment was fitted to one beam and the model was fitted to the other, so that each could be moved independently of the other.

A frame for the PIV system was built around one test beam, using extruded aluminium sections. The laser was oriented normal to the direction of motion, so that the measurement plane was across the direction of motion for the undisturbed flow. The borescopes for the CCD cameras were mounted symmetrically, approximately 650mm either side of the laser sheet. Camera 1 was upstream of the laser sheet, and Camera 2 was

downstream. The centre of the measurement window was approximately 950 mm away from the under the water optical unit for the laser. At no time during the testing were these positions changed. The minimum separation between the beams of the test frame was 922 mm. The final arrangement of the PIV system on the Ice Tank carriage test beam is shown in Figure 3.

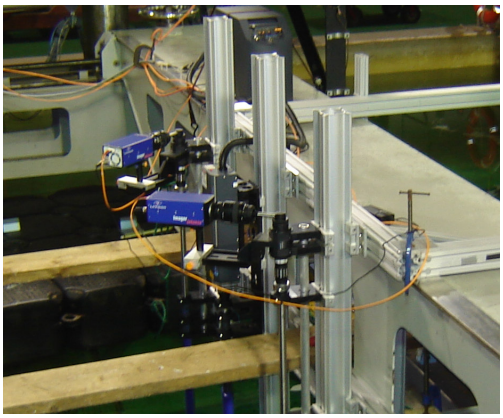

Figure 3, PIV system attached to towing carriage in the IOT Ice Tank

The model was connected to the carriage by two vertical, cylindrical poles and a yaw table. This yaw table enabled the yaw angle to be adjusted from zero to ninety degrees, in five-degree increments. The model hull was rigidly connected to the towing carriage, by bolting the yaw table around the carriage beam. To adjust the position of the model, relative to the laser sheet, the bolts around the beam were slacked off and the model slid forwards or backwards as required until the laser sheet was directed at the correct target on the model. The model and the assembled PIV system are shown in Figure 4.

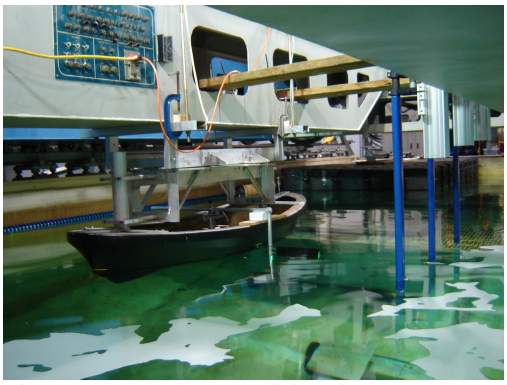

Figure 4, Escort tug model and PIV system attached to towing carriage in the IOT Ice Tank (model shown at zero yaw angle).

In order to calculate the 3-dimensional flow vectors, in-situ calibration of the measurement space was carried out prior to testing using a Type 30 calibration plate, supplied by LaVision GmbH. During calibration, the top of the plate was level with the waterline. The plate was adjusted until it was aligned with the laser sheet. The calibration was carried out using visible light, following the procedures required in the DaVis 7.1 software [9, 10].

For each data collection run, the sequence was to turn on the seeding system as the carriage started to move. PIV image data was collected for 50 or 100 image pairs once the carriage had reached a steady speed. On completion of data collection, the carriage was stopped and returned to its initial position. When all data at one measurement window location had been obtained, the beam with the model or the beam with the laser was moved to the new position.

Some routine checks were performed throughout the test program. Prior to the start of testing each day, the focus of each camera was checked. This was done by seeding the measurement space when the carriage was stationary and if necessary, adjusting the focus of the borescopes. In order to keep the PIV system optics clean, the borescopes and the laser tube were raised out of the water at the end of each day's testing. The optical parts were then washed with fresh water and lens cleaner to prevent the build-up of dirt.

Seeding the flow proved to be the most challenging aspect of carrying out these experiments. The CFD predictions suggested that the most important flow patterns were caused by the fin, and occurred under the hull towards the downstream side. For regions close to the hull, a three-fingered vertical rake was used. A typical installation is shown in Figure 5a). The flow in this region was unsteady, with quite abrupt changes in direction. As a result, locating the seeding rake was largely a matter of trial and error. The final location of the seeding rake for each measurement window had to be far enough upstream that the wake from the rake had stabilized, but close enough that the required concentration of particles was obtained across a large enough part of the measurement window. This position varied depending on the flow conditions and the location of the measurement window relative to the tug.

For locations close to the hull surface, but well below the free surface a 3-fingered horizontal rake was used. The shape of this rake allowed it to be positioned well under the model. This rake could be used for seeding from the upstream or downstream side of the model. Upstream seeding was used when the measurement window was under the hull, and close to the centreline of the hull.

Downstream seeding was used when the measurement window was on the downstream side of the hull at the deepest locations for the measurement window. A typical location for seeding on the downstream side of the model is shown in Figure 5b).

As the measurement window was moved to be further away from the model, the type of rake chosen was less critical. Any of the rakes could be used for measurements in these regions, and Figure 5c) shows the 3-fingered horizontal rake located for seeding a measurement area well away from the model.

The complete flow pattern for the area of interest around the escort tug model was larger than a single window of the PIV system. Extending the measurement area beyond a single window required several horizontal movements of the model and two depths of submergence for the PIV system within each plane. The increments of model movement in each direction were approximately one third of the dimension of the window (100mm). As a result a small area of the flow, relative to the model, should occur in at least three separate measurement windows.

The first step in the process of combining all the data within a measurement plane was to add the shift of the model (relative to the PIV measurement space) to the x and y coordinates obtained from the PIV window. The flow patterns obtained from different measurement windows at the same coordinates in the measurement plane were then compared. This was done by plotting the overlapped windows and comparing the measured velocity components. In general, the agreement between flow measurements for overlapped windows was very good, even when the flow conditions were highly unsteady.

a), Seeding location close to hull and free surface

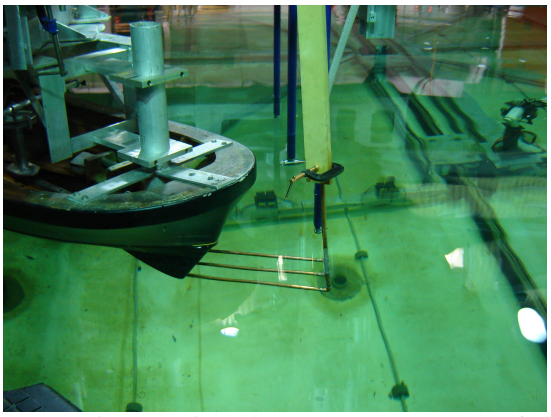

b), Seeding location close to hull but below free surface

c), Seeding location far from hull

Figure 5, Typical locations of seeding rake during experiments

The PIV data from the combined windows were plotted as contours of velocity component (V_x, V_y, V_z). The contour values were interpolated on a larger scale grid, which extended over the full measurement space. The interpolated velocity components were re-combined into three-dimensional vectors and compared with the original data to check for any significant errors or discrepancies. The data interpolation was carried out using *IGOR* [11]. The grid size for interpolating the experiment results can be chosen depending on the nature of the flow being studied. For all the cases given here, the grid spacing presented was on 20mm squares. The same technique was used to interpolate the CFD data, and the same grid was used for comparing the experiment results with the flow patterns predicted by CFD.

4. DISCUSSION

4.1 Upstream Side

The CFD predictions and the PIV experiment results for the in-plane flow vectors on the upstream side of the hull are shown in Figure 6. The main features of the experiment results and the CFD simulations were the flow away from the hull surface in the region close to the hull and the waterline, the separation of the flow from the upstream bilge corner and the upstream flow component close to the underside of the hull.

Overall, for the upstream side of the hull the CFD predicted the main features of the observed flow patterns. The worst predictions of the flow vectors were close to the hull and the accuracy of the predictions improved as the distance from the hull increased. PIV measurements close to the hull were the most difficult to obtain accurately, because the hull, even when painted black, reflected the light and a bright band was seen where the laser beam cuts the hull. Even though the analysis software included a filter to reduce this effect, the experiment results obtained in this region may be subject to error.

4.2 Downstream Side

The CFD predictions and the PIV experiment results for the in-plane flow vectors on the downstream side of the hull are shown in Figure 7. Both data sets show the presence of a well-defined vortex located under the bilge corner, which extends the full depth of the combined PIV measurement window. A second flow feature is the separation of the flow from this vortex when in interacts with the downstream bilge corner.

On the downstream side, the CFD predictions showed relatively small errors in the flow around the vortex. The worst comparison between the experiment data and the CFD predictions occurred close to the hull on the downstream side between the bottom of the hull and the waterline and under the hull.

The results given here are only for a flow speed of 0.5 metres per second. Overall there was little change in the mean direction of the flow vectors with speed for the two speeds tested, but the magnitudes of the vector components changed with the undisturbed flow speed. The biggest difference was for the downstream side of the hull with the fin fitted. Here, the region of low speed flow extended further away from the hull at 1 m/s than at 0.5 m/s.

4.3 Numerical Analysis of the Difference Between CFD Predictions and Experimental Measurements of Flow Vectors

The difference between the vectors derived from the PIV experiments and the CFD simulations on the same *y, z* coordinate locations was calculated, using the expression

$$\overline{V_{error}} = \overline{V_{expt}} - \overline{V_{cfd}}$$

The following parameters were also used as part of the numerical evaluation of the difference between the experiment values and the CFD predictions:

$$ErrorV_x = Vx_{expt} - Vx_{cfd}$$
$$ErrorV_y = Vy_{expt} - Vy_{cfd}$$
$$ErrorV_z = Vz_{expt} - Vz_{cfd}$$

$$Error_{2D} = \sqrt{ErrorV_y^{\,2} + ErrorV_z^2}$$
$$Error_{3D} = \sqrt{ErrorV_x^2 + ErrorV_y^2 + ErrorV_z^2}$$

The results of the numerical analysis are summarized in Tables 4 and 5. The numerical methods for comparing the CFD predictions and the experimental measurements have been described in more detail [12].

The numerical analysis showed that the mean error in the in-plane vectors between the CFD predictions and the experiments was 0.038 m/s on the upstream side and 0.051 m/s on the down stream side. As fractions of the free-stream speed, these were 7.6% with a standard deviation of 10.6% and 10.2% with standard deviations of 7.4% respectively. The number of data points where the error between the CFD prediction and the experiment was less than 10% of the free stream speed was 84% for the upstream side and 60% for the down stream side. The flow on the downstream side was much more turbulent than on the upstream side [13].

From this analysis it can also be seen that the value of *Error Vx* is consistently negative. This means that the flow component from the CFD predictions was consistently higher than the observed values in the experiments. The difference was consistent with the values of the wake from the seeding rake used for these experiments [8], which was seen to be between 10 and 12 percent of the free stream flow. It was expected that the wake from the seeding rake was reducing the flow speed, relative to the case when the rake was not present. It was also shown that the rake had negligible effect on the in-plane flow measurements, so comparison between the CFD simulations and the PIV experiments should be focussed on the in-plane flow patterns.

6. CONCLUSIONS

A commercial CFD code can be used to predict the flow patterns around a hull at a yaw angle larger than those typically encountered during manoeuvring. The CFD code predicted that the flow separated on the upstream side of the hull at the bilge and a vortex was formed under the hull. On the downstream side of the hull, the CFD code predicted a large vortex is formed by the fin, which extended from the waterline to well below the combined depth of the hull and fin. A secondary flow feature on the downstream side was the separation of flow around this vortex on the downstream bilge. The predictions were confirmed by the PIV measurements. The CFD simulations were presented for a mesh that was composed entirely of elements constructed of six four-sided faces.

The PIV measurements showed that the average error between the CFD predictions and the experiments was 7.6% on the upstream side and 10.6% on the downstream side of the hull. These levels of agreement were within the estimated uncertainty of the PIV system measurements for the arrangement of components that was used for these experiments. This observation leads to the conclusion that a commercial CFD code can be used to predict the magnitude and direction of the flow vectors around an escort tug hull at a yaw angle of 45 degrees.

If the CFD code accurately predicts the flow patterns at a yaw angle of 45 degrees, it can be surmised that other yaw angles can be studied by CFD alone.

7. ACKNOWLEDGEMENTS

The work described in this paper would not have been possible without the help and support of many people, which is gratefully acknowledged:

Mr. Robert Allan, President of Robert Allan Ltd., Vancouver, British Columbia, gave permission to use the model of the escort tug in the PIV experiments and CFD simulations.

The Canada Foundation for Innovation and the Newfoundland and Labrador Department of Innovation, Trade and Rural Development provided financial support of the purchase of the PIV system used for the escort tug experiments.

Mr. Jim Gosse, Laboratory Technician in the Fluids Laboratory at Memorial University helped during the preliminary PIV experiments.

The staff at IOT for prepared the model and assisting with the many tasks required during experiments at IOT.

The management of IOT provided financial support for the project, which included the first author obtaining a Ph.D. based on this research.

8. REFERENCES

1. Hutchison, B., Gray, D. and Jagannathan S., 'New Insights into Voith Schneider Tractor Tug Capability', *Marine Technology*, Vol. 30, No. 4, pp. 233-242, 1993.

2. Allan, R. G, Bartells, J-E. and Molyneux, W. D. 'The Development of a New Generation of High Performance Escort Tugs', Proceedings,

International Towage and Salvage Conference, Jersey, May 2000.

3. Allan R. G. and Molyneux, W. D. 'Escort Tug Design Alternatives and a Comparison of Their Hydrodynamic Performance', Trans. S. N. A. M. E. Vol. 112, pp 191-205, 2004.
4. Molyneux, W. D. 'A Comparison of Hydrodynamic Forces Generated by Three Different Escort Tug Configurations', NRC/IOT TR-2003-27.

5. Fluent Inc. 2005(b) 'Gambit 2.2 User's Guide', available on-line, June 2005. http://www.fluentusers.com/gambit/doc/doc_f.htm

6. Fluent Inc. 2005(a) 'Fluent 6.2 User's Guide', available on-line, July 2005. http://www.fluentusers.com/fluent/doc/ori/html/ug/main_pre.htm

7. Xu, J., Molyneux, W. D. and Bose, N. 'A Versatile PIV System for Flow Measurements in Water Tanks', 7th Canadian Marine Hydromechanics and Structures Conference, Halifax, N. S. September 2005.

8. Molyneux, W. D., Xu, J. and Bose, N. 'Commissioning a Stereoscopic PIV System for Application in a Towing Tank', Proceedings, 28th American Towing Tank Conference, Ann Arbor, Michigan, August 9-10th, 2007.

9. LaVision GmbH, 'DaVis Software Manual for DaVis 6.2', 2005.

10. LaVision Inc., 'DaVis Flowmaster Software Manual for DaVis 7.1', 2005.

11. Wavemetrics Inc. 'Igor Pro Version 5 Users Guide', 2004.

12. Molyneux, W. D. and Bose, N. 'A Quantitative Method to Compare Results from Different CFD simulations and Experimental Data', Submitted to Journal of Ship Research, SNAME, 2007.

13. Molyneux, W. D., Xu, J. and Bose, N. 'Measurements of Flow Around an Escort Tug Model With a Yaw Angle', accepted for publication, Marine Technology, S.N.A.M.E. 2007.

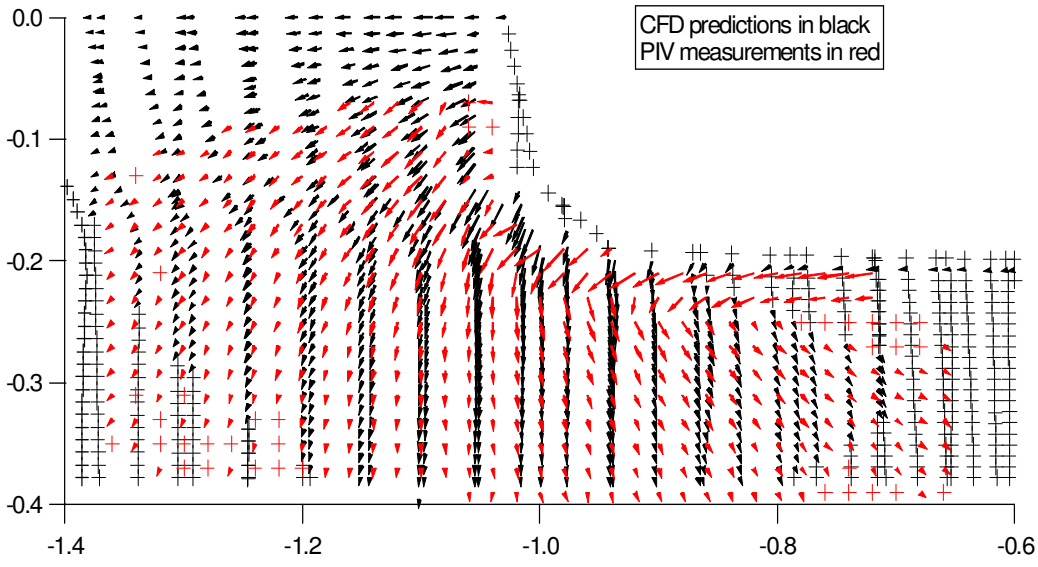

Figure 6, In-plane flow vectors, upstream side (no fin)

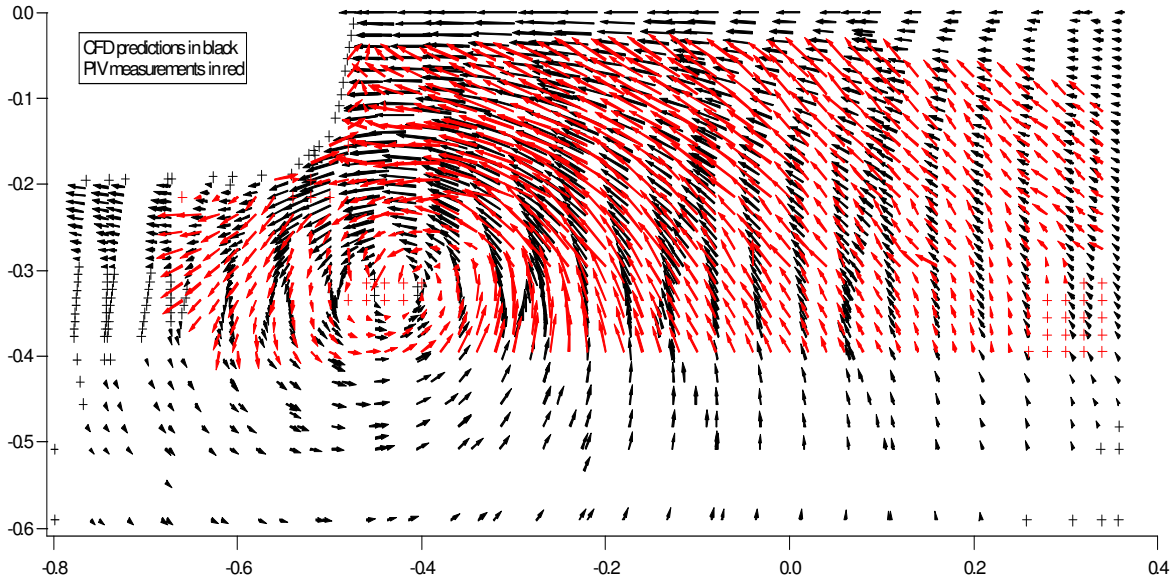

Figure 7, In-plane flow vectors, downstream side (with fin)

Table 4, Upstream side, no fin, summary of error in CFD prediction,
Flow speed 0.5 m/s

	Average	Standard Deviation	Minimum	Maximum	Range
In-plane	m/s	m/s	m/s	m/s	m/s
Error Vy	0.001	0.061	-0.282	0.136	0.418
Error Vz	0.001	0.023	-0.064	0.142	0.205
Error 2d	0.038	0.053	0.001	0.282	0.281
Through plane					
Error Vx	-0.069	0.041	-0.300	0.115	0.415
Error 3d	0.085	0.060	0.018	0.372	0.354

Table 5, Downstream side, with fin, summary of error in CFD prediction,
Flow speed 0.5 m/s

	Average	Standard Deviation	Minimum	Maximum	Range
In-plane	m/s	m/s	m/s	m/s	m/s
Error Vy	0.007	0.048	-0.128	0.278	0.406
Error Vz	0.021	0.034	-0.116	0.116	0.232
Error 2d	0.051	0.037	0.000	0.290	0.290
Through plane					
Error Vx	-0.088	0.052	-0.200	0.278	0.478
Error 3d	0.113	0.039	0.034	0.388	0.354